Engineering Analysis with Boundary Elements 36 (2012) 1908–1916

Contents lists available at SciVerse ScienceDirect

Engineering Analysis with Boundary Elements

journal homepage: www.elsevier.com/locate/enganabound

Stress analysis of solids with open-ended tubular holes by BFM

Cheng Huang, Jianming Zhang *, Xianyun Qin, Chenjun Lu, Xiaomin Sheng, Guangyao Li

State Key Laboratory of Advanced Design and Manufacturing for Vehicle Body, College of Mechanical and Vehicle Engineering, Hunan University, Changsha 410082, China

ARTICLE INFO

Article history:
Received 3 May 2012
Accepted 15 July 2012

Keywords:
Stress analysis
Tubular hole
Boundary face method

ABSTRACT

Two kinds of special surface elements, curvilinear tube element and triangular element with negative parts, are proposed for modeling solids containing many slender open-ended tubular shaped holes in the framework of boundary face method. The surfaces of each tubular hole in the solid are modeled by the tube elements, and the outer surfaces that intersected and trimmed by the holes are modeled by triangular elements with negative parts. Substantial savings in both modeling effort and computational cost have been achieved. In addition, all the special surface elements are defined in the parametric space of the surface, and the exact geometry data are obtained directly from a CAD model of the solid. Therefore, automatic analysis is possible. Several numerical examples are presented to demonstrate the efficiency and accuracy of the proposed method.

1. Introduction

The problem of calculating the displacement and stress field in elastic solids containing many small holes is of considerable interest in engineering. For instance, in construction process of concrete dams many slender holes are designed as cooling passages. And these small holes can significantly change the stress distribution in dams. The analysis of solids with small holes is still a difficult task by finite element method (FEM), as the FEM requires a very fine mesh to make sure the accuracy of the result. Usually, very large amount of modeling efforts are necessary for mesh generation in a body with many small holes, especially when the holes are very small in size.

Compared to the finite element method, the boundary element method is more suitable for this task. Because the BEM can reduce the dimensionality of the problem, and only need to mesh the surface of the domain. A number of boundary element methods have been developed and implemented for heat conduction and elastic stress analysis of the solids with small holes and fibers [1–7]. The method developed by Henry, Banerjee and Chatterjee [1–5] proposed a boundary element formulation for the efficient modeling and analysis of tubular holes, reducing both the amount of data and computational cost of conventional BEM formulation. The variations in the circumferential direction of the hole are represented in terms of a trigonometric shape function together with a linear or quadratic variation in the longitudinal direction. The resulting integrals are treated semi-analytically. Federico proposed a boundary element formulation using a single special hole element for modeling two-dimensional microstructures containing cylindrical voids. And a family of hole elements with 3, 4, 5 and 6 nodes is presented [7].

In the present paper the boundary face method (BFM) [8] is introduced to readily analyze elastic problem of three-dimensional solids with small tubular shaped holes of free shape. The BFM is implemented directly based on the boundary representation data structure (B-rep) that is used in most CAD packages for geometry modeling. Each bounding surface of geometry model is represented as parametric form by the geometric map between the parametric space and the physical space. Both boundary integration and variable approximation are performed in the parametric space. The integrand quantities are calculated directly from the faces rather than from elements, and thus no geometric error will be introduced [9]. The hole with complex geometries, such as the sharp variation of the curvature along its length and the arbitrary shaped cross section, can be easily represented by BFM. Thus, our method not only can analyze the straight cylindrical holes but also the hole of free shapes.

We present a tube element and a triangular element with negative parts to model the surface of the problem domain with open-ended tubular holes. These holes can be modeled by special tube elements. Therefore the discretization of the surface is very simple, resulting in substantial savings in both data preparation and computing costs. In the previous work, those methods used for this problem treated solid and holes as separate regions and the ends of the hole are closed by a circular disc. However, in our method with these special surface elements the solid and holes are modeled as one region. These holes are open-ended, and intersect the outer surface of the body. So, our method can reduce both the modeling and computational task significantly with using these two Special surface elements.

* Corresponding author. Tel.: +86731 88823061.
E-mail address: zhangjianm@gmail.com (J. Zhang).

0955-7997/$ - see front matter © 2012 Elsevier Ltd. All rights reserved.
http://dx.doi.org/10.1016/j.enganabound.2012.07.009

In this work, both the integrals over the surfaces of the holes and the surfaces of the domains are computed numerically different from semi-analytically as in the previous works. The numerical evaluation of the boundary integrals plays a key role in the implementation of the BFM. Therefore, special treatments of the integrals with nearly singularities and singularities are designed, which will be discussed in the following section of this paper.

In the following sections, Section 2 describes the boundary integral equation formulation for elastic stress analysis with open-ended tubular holes. Special surface elements for modeling open-ended tubular holes are described in Section 3. In Section 4, the issues for numerical integrations are discussed. Several numerical examples are provided in Section 5. And the paper ends with conclusions in Section 6.

2. Boundary integral equation formulation with open-ended tubular holes

The BFM is a new implementation of the boundary node method (BNM) or BEM [8–13]. For the method, the boundary consists of a set of surfaces with parametric representation and the field variable approximation is performed in parametric space of each surface. The parametric surface is discretized by surface elements in parametric space. These elements are used for the boundary integration and variable approximation. The details of the implementation for the BFM can be found in Refs. [8,9].

The self-regular BIE for elastic stress analysis of a body containing open-ended tubular holes can be expressed as

$$0 = I^O + I^H + I^V \tag{1}$$

where

$$I^O = \int_{\Gamma^O} [(u(\mathbf{s}) - u(\mathbf{y}))T(\mathbf{s},\mathbf{y}) - t(\mathbf{s})U(\mathbf{s},\mathbf{y})]d\Gamma^O(\mathbf{s}) \tag{2}$$

$$I^H = \sum_{m=1}^{M} \int_{\Gamma_m^H} [(u(\mathbf{s}) - u(\mathbf{y}))T(\mathbf{s},\mathbf{y}) - t(\mathbf{s})U(\mathbf{s},\mathbf{y})]d\Gamma_m^H(\mathbf{s}) \tag{3}$$

$$I^V = \sum_{k=1}^{K} \int_{\Gamma_k^V} [(u(\mathbf{s}) - u(\mathbf{y}))T(\mathbf{s},\mathbf{y}) - t(\mathbf{s})U(\mathbf{s},\mathbf{y})]d\Gamma_k^V(\mathbf{s}) \tag{4}$$

in which:

u and t are boundary displacement and traction;

$\mathbf{y}$ is the source point and $\mathbf{s}$ is the field point on the boundary;

U and T are the fundamental solutions of the 3D elastic problems;

Γ_m^H is the surface of the mth hole;

Γ_k^V is the kth special element with negative parts created by open-ended holes;

Γ^O is the out surface of the body exception for the special elements;

I^O denotes the integrals over the Γ^O;

I^H and I^V denote the integrals over the summation of the Γ_m^H and Γ_k^V, respectively;

M and K are the total number of the holes and the elements with negative parts, respectively.

The boundary element discretization of this problem in the conventional manner requires a very fine mesh about the hole. In this work, the discretization of the solid with small holes is very simple, because an efficient boundary face element with special surface elements is introduced for the efficient modeling and analysis of the holes. The geometric information of the hole is directly derived from its parametric surface of its CAD model [9]. This is a distinguishing advantage over the BEM, in which the surface elements are defined in physical space, and the hole is approximated by those elements.

In the previous work, the hole element is closed at the end by a circular disc and those method used for this problem treated solids and holes as separate regions. The hole concerned in this paper is open-ended, and intersects the outer surface of the body. The treatment for this type of hole is troublesome and uneconomical in the BEM, and so far no literatures are found about dealing with those holes. The boundary face method is introduced in this paper for the efficient modeling and analysis of holes using boundary elements with negative parts created by open-ended holes. The special surface elements will be described in the next section.

3. Special surface elements for modeling of open-ended tubular holes

As mentioned previously, the hole which is open-ended and intersects the outer surface of the body can be efficient modeled and analysis by using the slender tube element and the special triangular element with negative parts. In this section, the tube element and the special triangular element with negative parts are detailed described.

3.1. Tube element

In previous work, the holes are modeled in three-dimensional space using 'hole elements' with a prescribed radius. The holes assume a variation in the displacement field about the circumference defined by a trigonometric function, and a linear or quadratic variation is assumed along its length [1]. However, a hole is represented exactly by several tube elements in our work, not approximated with hole elements. The hole is described by slender surface elements in parametric space. This kind element is referred to as 'tube element' here, which is different from the 'hole element' mentioned in previous work. A slender hole modeled with four tube elements is shown in Fig. 1. Each tube element is composed of four isoparametric lines in the parametric coordinate (u, v) of the surface as illustrated in Fig. 2(a). In the space, v is along tube's longitudinal direction, while u is along the circumferential direction taking a value from 0 to2π.

To perform numerical integration, the following linear transformation is applied to mapping a tube element into a normalized space denoted by the local coordinate system (ξ, η).

$$\begin{cases} \xi = (u - u_0)/a \\ \eta = (v - v_0)/b \end{cases} \quad \xi,\eta \in [0,1] \tag{5}$$

where

$$\begin{cases} u_0 = (u_2 + u_1)/2 \\ v_0 = (v_1 + v_2)/2 \end{cases} \text{ and } \begin{cases} a = (u_2 - u_1)/2 \\ b = (v_2 - v_1)/2 \end{cases}$$

A type of the discontinuous tube elements is used. The interpolating nodes are not shared in neighbor elements, thus the variation of approximated field variable is discontinuous among these elements. For each element, interpolating nodes are symmetrically distributed inside it, as showed in Fig. 2(c). There is an offset between each node and the associated element

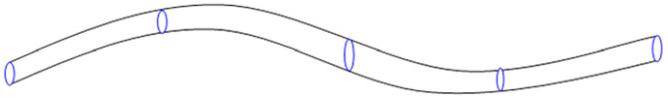

Fig. 1. A hole modeled by four tube elements.

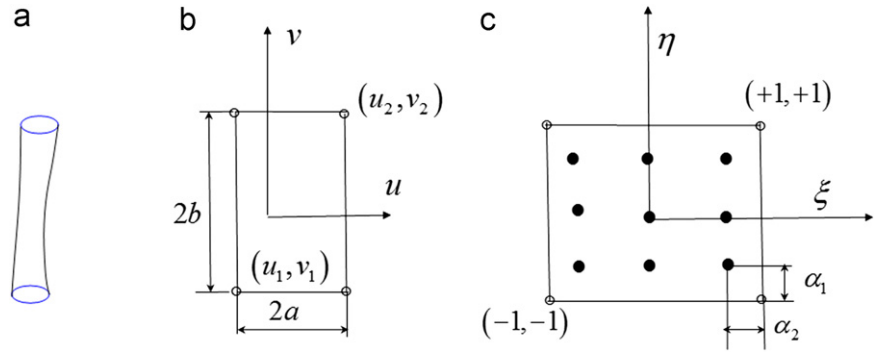

Fig. 2. A tube element, '○' denotes an element vertex and '●'denotes an interpolating node. (a) Element in physical space; (b) Element in parametric space of the surface; (c) Element mapped into a local coordinate system.

vertex. And the location of the node is determined by two offset parameters, α_1 and α_2. In this paper, α_1 and α_2 are specified as 1/3 and 1/4, respectively. As in Ref. [1], the resulting displacements are described by using a trigonometric circular shape function in the circumferential direction and a curvilinear shape function of any order in the longitudinal direction. In the circumferential direction, the following transformation from ξ to u is required for using the circular shape functions in Ref. [1].

$$u = \frac{2\pi^*(\xi+1.0)}{2} - \frac{\pi}{3} \tag{6}$$

Using this transformation, the circular shape functions can be expressed as

$$\begin{aligned} M^0(u) &= \frac{1}{3} + \frac{2}{3}\cos u \\ M^1(u) &= \frac{1}{3} + \frac{\sqrt{3}}{3}\sin u - \frac{1}{3}\cos u \\ M^2(u) &= \frac{1}{3} - \frac{\sqrt{3}}{3}\sin u - \frac{1}{3}\cos u \end{aligned} \tag{7}$$

In the longitudinal direction, if a quadratic variation is taken, the shape functions are represented as

$$\begin{aligned} N^0 &= -0.5\beta(1-\beta) \\ N^1 &= 0.5\beta(1+\beta) \\ N^2 &= (1+\beta)(1-\beta) \end{aligned} \tag{8}$$

where

$$\beta = \frac{\eta}{1.0-\alpha_2}, \quad \alpha_2 \in (0,1)$$

As in Ref. [2], the displacement on the hole varies in the longitudinal as well as circumferential direction. The displacement variations can be expressed as

$$u = M^{\alpha}(\mathbf{s})N^{\gamma}(\mathbf{s})u^{\alpha\gamma} \tag{9}$$

After dividing the mth hole into N_M number of tube elements together with using the shape functions mentioned above, Eq. (3) can be discretized as

$$\begin{aligned} I_m^H = &\sum_{i=1}^{N_M} \int_{\Gamma_{mi}^H} T(\mathbf{s},\mathbf{y})[M^{\alpha}(\mathbf{s})N^{\gamma}(\mathbf{s}) - M^{\alpha}(\mathbf{y})N^{\gamma}(\mathbf{y})]u^{\alpha\gamma} d\Gamma_{mi}^H(\mathbf{s}) \\ &- \sum_{i=1}^{N_M} \int_{\Gamma_{mi}^H} U(\mathbf{s},\mathbf{y})M^{\alpha}(\mathbf{s})N^{\gamma}(\mathbf{s})t^{\alpha\gamma} d\Gamma_{mi}^H(\mathbf{s}) \end{aligned} \tag{10}$$

in which the subscripts mi is used to denote the ith tube element over the mth hole, $u^{\alpha\gamma}$ and $t^{\alpha\gamma}$ are nodal values of displacements and tractions on the surface of the tube element. Summation over α and γ is implied. α ranges from 1 to the number of nodes in circumferential direction, and γ ranges from 1 to the number of nodes along the longitudinal direction of the hole.

It should be noticed that no geometric approximation is performed in Eq. (10). For obtaining exact geometry, at first we obtain the surface parametric coordinates u and v from local integration points using Eq. (5), and then the geometric data is directly calculated from the parametric surface with the parameters: u and v. The calculation is completed using the parametric formulation of the surface, which is available from its B-rep data of the CAD model.

3.2. Triangular elements with negative parts

In the present work, the hole is open-ended and intersects the outer surface of the body, so the surface is trimmed with small holes. The boundary element discretization of this problem in the conventional method requires a very fine mesh about the hole. To avoid using a fine mesh to describe each hole, a class of new discontinuous triangular elements with negative parts is developed in this section. The local region of the surface around the hole can be meshed with a fewer of those elements instead of a large number of traditional elements, as shown in Fig. 3. The hole is decomposed as several negative parts, which are located at the corners of the triangular elements with negative parts. The radius of a negative part is equal to the radius of the hole. The center of the hole is coincident with one of the vertices of those elements. Before mesh generation, all centers of the holes are set as hard points, which are the locations of the nodes of the final mesh. The task of meshing the surface with hard points can be completed in an easy manner with existing meshing techniques. This is why the negative parts are located at the corners of the elements, not inside them. In the case where a large number of holes are present, the elements with negative parts can be generated much more efficiently than the traditional method.

Fig. 4 shows a triangular element with two negative parts in different spaces. The small negative parts are not drawn in Figs. 4(b) and 4(c). The element is defined in the surface parametric space (u, v) by three or six vertices with parametric coordinates as shown in Fig. 4(b). And Fig. 4(c) depicts the element in the local coordinate system (ξ, η) mapped from the space (u, v). If there are three vertices employed, the following mapping is used from the space (ξ, η) to (u, v).

$$\begin{cases} u = \sum_{i=1}^{3} \phi_i(\xi,\eta)u_i \\ v = \sum_{i=1}^{3} \phi_i(\xi,\eta)v_i \end{cases} \tag{11}$$

in which $\phi_1 = \xi$, $\phi_2 = \eta$ and $\phi_3 = 1-\xi-\eta$. Naturally, when six vertices are involved, the quadratic functions of ϕ_i can be available, where i from 1 to 6.

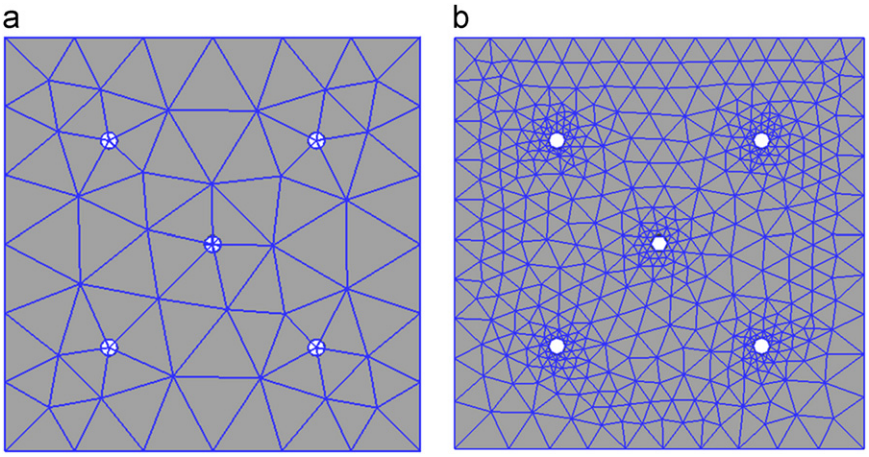

Fig. 3. The two type of meshes for the surface with five small holes. (a) Triangular elements with negative parts. (b) Traditional triangular elements.

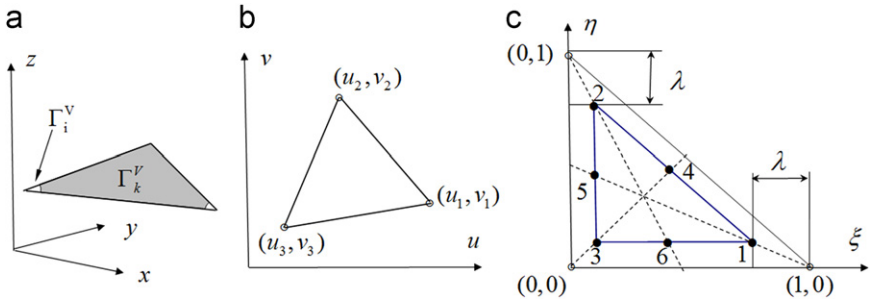

Fig. 4. A triangular element with negative parts. (a) Element in physical space. (b) Element in parametric space of the surface. (c) Element mapped into a local coordinate system.

Three interpolating nodes are used for linear interpolation of field variables. These nodes are located at midlines of the triangular element. An offset from the associated element vertex is taken to locate each node, and the node location is determined by an offset parameter λ. These three nodes are shown in Fig. 4(c) with indices of 1, 2, and 3. The local coordinates of the nodes are set by $(1-\lambda,0.5\lambda)$, $(0.5\lambda, 1-\lambda)$ and $(0.5\lambda, 0.5\lambda)$, respectively. λ is constrained as the interval (0.1, 0.4) based on our experience. λ is specified as 0.3 in this paper. The triangular patch constructed with the inner nodes is similar to the triangular element. Thus, the linear interpolating shape functions associated with three interpolating nodes can be expressed as

$$\varphi^1 = \frac{1}{1-1.5\lambda}(\xi-0.5\lambda)$$
$$\varphi^2 = \frac{1}{1-1.5\lambda}(\eta-0.5\lambda)$$
$$\varphi^3 = \frac{1}{1-1.5\lambda}(1-\xi-\eta-0.5\lambda) \tag{12}$$

Similarly, the quadratic shape functions with six nodes can be easily obtained as

$$\varphi^1 = a(2a-1)$$
$$\varphi^2 = b(2b-1)$$
$$\varphi^3 = (1-a-b)(2(1-a-b)-1)$$
$$\varphi^4 = 4ab$$
$$\varphi^5 = 4b(1-a-b)$$
$$\varphi^6 = 4a(1-a-b) \tag{13}$$

in which $a = \frac{1}{1-1.5\lambda}(\xi-0.5\lambda)$ and $b = \frac{1}{1-1.5\lambda}(\eta-0.5\lambda)$. The locations and indices of the six nodes are also shown in Fig. 4(c).

Using the shape functions mentioned above, Eq. (4) for the kth element with N_K number of negative parts can be expressed as

$$I_k^V = \int_{\Gamma_s^V}[T(\mathbf{s},\mathbf{y})(\varphi^\gamma(\mathbf{s})-\varphi^\gamma(\mathbf{y}))u^\gamma - U(\mathbf{s},\mathbf{y})\varphi^\gamma(\mathbf{s})t^\gamma]d\Gamma_s^V(\mathbf{s}) - \sum_{i=1}^{N_K}\int_{\Gamma_i^V}[T(\mathbf{s},\mathbf{y})(\varphi^\gamma(\mathbf{s})-\varphi^\gamma(\mathbf{y}))u^\gamma - U(\mathbf{s},\mathbf{y})\varphi^\gamma(\mathbf{s})t^\gamma]d\Gamma_i^V(\mathbf{s}) \tag{14}$$

where the subscripts s and i refer to the region of the whole element and the region of the ith negative part of the element, respectively, u^γ and t^γ are nodal values of displacements and tractions on the surface of the element. Summation over γ is implied, where γ ranges from 1 to the number of the nodes in the kth element.

In Eq. (14), at first, the initial integrals over the whole triangular element are computed. Then, the final integrals over the surface region on the element are calculated by subtracting the integrals in all negative parts from the initial integrals. In the computing process, the same shapes functions from Eqs. (12) or (13) are used.

4. Numerical integration of the coefficient matrix

The accuracy of the BFM is critically depending on the correct evaluation of boundary integrals. In this work, all regular integrals of the formulation are evaluated numerically using the regular Gaussian integration. The non-regular integrals may present various degrees of singularity, and they are treated as follows.

When y and s belong to different element, they can still be very close to each other. Then, the integrals on the right hand side of

Eq. (14) become nearly singular. We have developed an adaptive integration scheme based on adaptive element subdivision method to calculate nearly singular integrals. The details of this method can be found in Refs. [8,9].

The term with $T(s, y)$ on the right hand side of Eq. (14) contains strongly singular kernels, which are calculated in an indirect way by using the rigid body displacement technique. The term with $U(s, y)$ on the right hand side of Eq. (14) becomes a weakly singular integral when y and s belongs to a same element.

To calculate the weakly singularity integral, we have developed a new coordinate transformation based on a triangle, and the details of the method can be found in Ref. [9]. Before using this technique, the element under integration has to be subdivided into several triangles. In the case where a regular quadrilateral element is involved and the source point y is located at the center of the element, the element will be divided into four nearly equilateral triangles. This subdivision is reasonable for obtaining accurate numerical integrals over the whole element.

However, in the cases where the element is very irregular or the source point is close to the edges of the element. The above subdivision is no longer suitable. In these cases, the element is divided into several triangles and additional quadrangles. For each triangle, the singular integrals are calculated by using the mentioned coordinate transformation, while for the quadrangles, nearly singular integrals are calculated by the adaptive integration scheme [9]. The subdivision is implemented by the following three steps.

- First, compute the arc lengths of the parametric lines form the source point y to each edge of the element and obtain the minimum length d, in the real-world-coordinate system.
- Then, based on d, we construct a rectangular box in the element local coordinate system, but with possibly the square shape in the real-word-coordinate system, and resulting in y at the center of the box.
- Finally, triangles are constructed from the box and additional quadrangles are created from the remained region of the element.

Applying the above strategy, subdivisions of three different kinds of cases are shown in Fig. 5. We can see that the subdivision of each case is dependent on the element shape and the location of the source point. The subdivision of a slender tube element is similar to that shown in Fig. 5(b) or Fig. 5(c), regarding to the location of source point.

For discontinuous triangular elements, we also have developed a special subdivision scheme. The subdivision is carried out based on two general cases. In the first case, the source point is close to a corner of the element. In the second case, the source point is close to the middle of an element edge. Fig. 6(a) and (b) show the subdivisions of the same element in these two cases, respectively. The whole element is divided into several triangles depending on the location of the source point. Over the triangles with a vertex of the source point, weakly singular integrals are calculated by the coordinate transformation technique [9]. For the others, the integration is performed by the adaptive subdivision scheme [9].

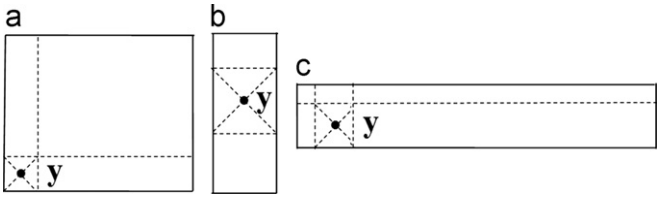

Fig. 5. Subdivisions of three quadrilateral elements. (a) A square element with source point near its corner. (b) A slender element with source point near its center. (c) A much slender element with source point near its corner.

5. Numerical applications

In this section, in order to assess the efficiency and accuracy of the proposed method some numerical examples are presented.

5.1. Block with a hole

The first example is a block with a cylindrical hole. It is used to demonstrate the capacity of capturing the stress concentration of the proposed method. It is a $10 \times 10 \times 4$ block with an open-ended cylindrical hole. The slender hole is vertical to the bottom face $z=0$ of the block. The central line of the hole passes through the block's center with coordinates (5, 5, 2). Two kinds of cases of the problems are handled regarding to different diameter of the hole.

In the first case, the diameter is taken as 0.4. The Young's modulus is 10,000 and the Poisson's ratio is 0.25. The block is submitted to uniform traction of 100.0 with the face $y=10$ and it is supported with the face $y=0$, as shown in Fig. 7. This problem is solved by the proposed method. For comparison, the traditional BFM without new proposed elements is also carried out for the same problem. The BFM boundary meshes with proposed elements are shown in Fig. 8. Fig. 9 shows the meshes used in the traditional BFM. We can see that the mesh of the proposed method is much simpler than the mesh used in the traditional BFM.

All computations have been performed in the same integration schemes. In each computation, the numerical results of stress in three dimensions at the internal locations are evaluated. These locations are uniformly distributed on the line with ends (0.223, 5, 2) and (4.79, 5, 2), as shown in Fig. 7. All results are shown in Figs. 10 and 11. Fig. 10 shows the displacement component in x coordinate axis at internal locations calculated by these two methods. Fig. 11 shows the actual stress concentration up to a point close to surface of the hole is in very good agreement with those obtained by the traditional BFM. The variation of the stress and displacement obtained by the BFM with new proposed elements is in excellent agreement with that of the traditional BFM. In the present method, the total numbers of elements and

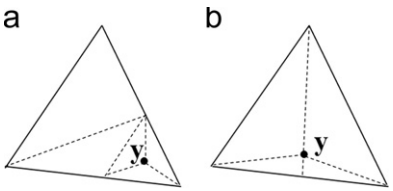

Fig. 6. Subdivisions of a triangular element. (a) Source point near an element corner. (b) Source point near the middle of an element edge.

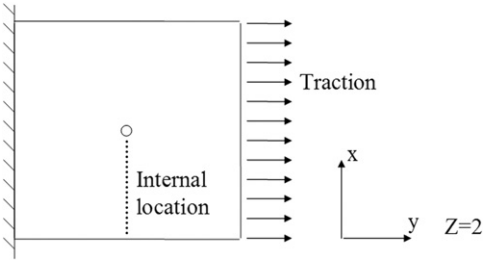

Fig. 7. Boundary conditions of the block.

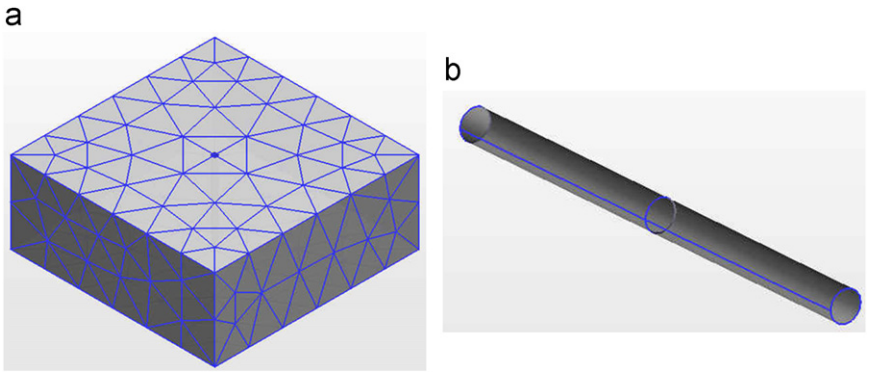

Fig. 8. BFM meshes with proposed elements for a block with a hole. (a) Overall boundary meshes with the number of elements 293. (b) The hole modeled with only two tube elements.

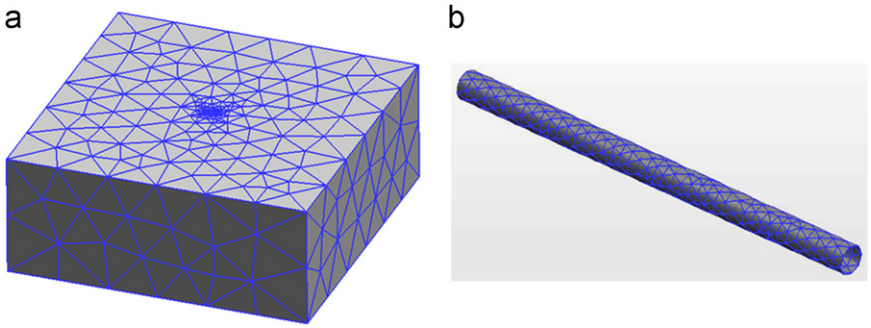

Fig. 9. BFM meshes with traditional elements for a block with a single hole. (a) Overall boundary meshes with the number of elements 1032. (b) The hole modeled with traditional elements.

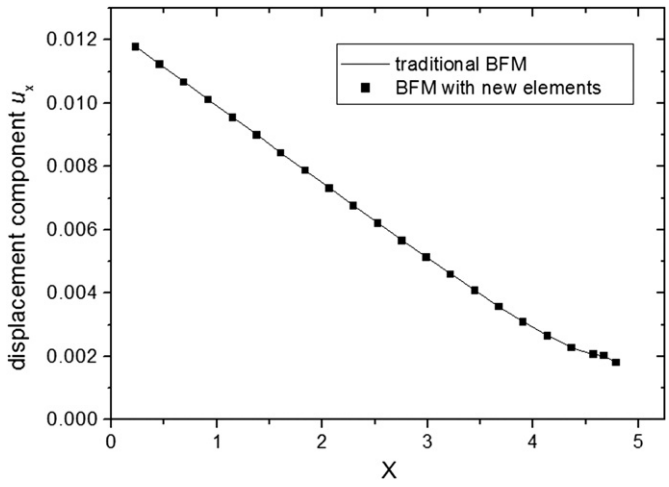

Fig. 10. Variation in displacement component in x coordinate axis at internal locations for a block with a hole of diameter 0.4.

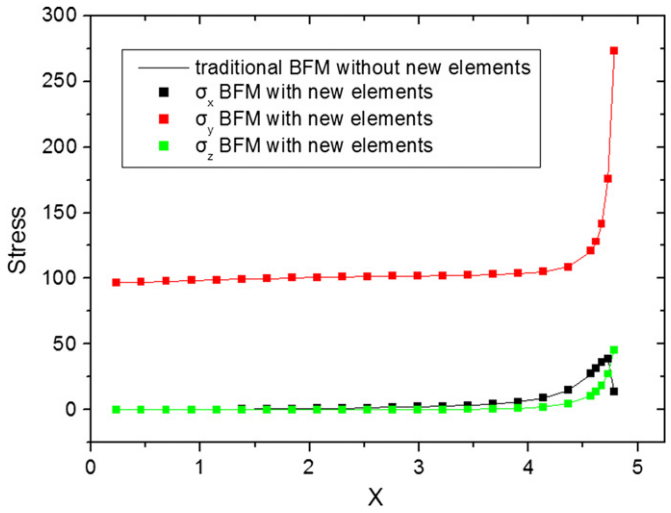

Fig. 11. Variation in stress at internal locations for a block with a hole of diameter 0.4.

nodes are 293 and 885, respectively, while in traditional method the related numbers up to 1032 and 3096, respectively.

In the second case, the diameter of the hole is specified as a small value 0.1, compared with the side length of the bock. This case is used to demonstrate the capacity of dealing with hole with very small radius. The boundary condition of this case is the same as the first case. In this case, the boundary mesh of the present method is the same as the first case. However, in traditional method the total numbers of elements and nodes are increase to 2146 and 6438. Again, the results at internal locations are calculated. These locations are uniformly distributed on the line with ends (0.223, 5, 2) and (4.94, 5, 2). All results are shown in Fig. 12. It is found that the same level of the accuracy is obtained by the present method, in which fewer elements are used when compared with the traditional methods.

5.2. Block with multiple holes

The second example consists of a $10 \times 10 \times 4$ block with five open-ended cylindrical holes, as shown in Fig. 13. The diameters of all the holes are set as 0.4. This example is considered here to show the advantage of our method in modeling of structures containing many open-ended tubular holes.

The boundary condition of this case is the same as the first example, as shown in Fig. 7. This problem is solved by the

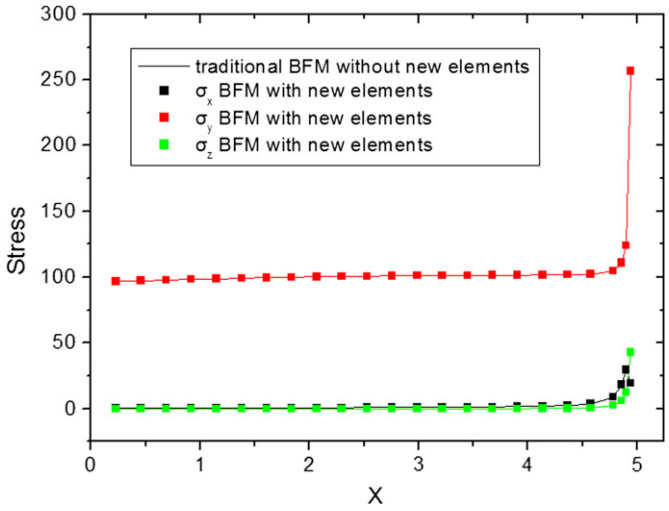

Fig. 12. Variation in stress at internal locations for a block with a hole of diameter 0.1.

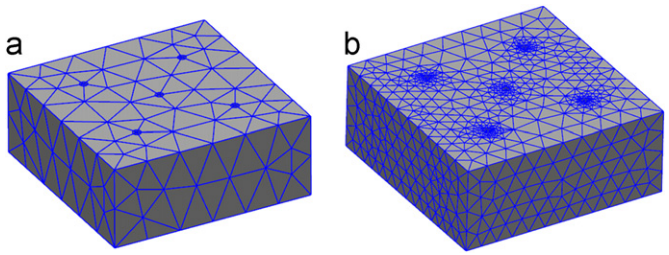

Fig. 13. (a) Meshes with proposed elements with the number of elements 301. (b) Meshes with traditional elements with the number of elements 4052.

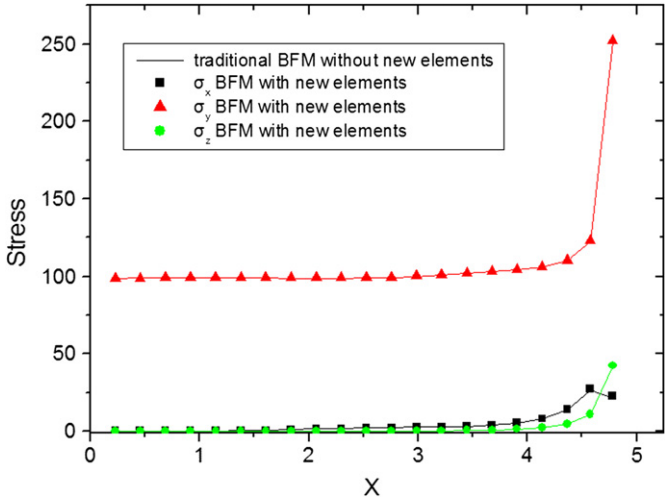

Fig. 14. Variation in stress at internal locations for a block with 5 holes of diameter 0.4.

proposed method and the traditional BFM without new proposed elements. The boundary meshes with proposed elements and the meshes used in the traditional BFM are shown in Fig. 13. For this example, we can see that the mesh of our method is much simpler than the mesh used in the traditional BFM. Therefore, the proposed method is much more efficient than the traditional BFM while there are more holes.

The results at the internal locations are calculated. All results are shown in Fig. 14. In the present method, the total numbers of

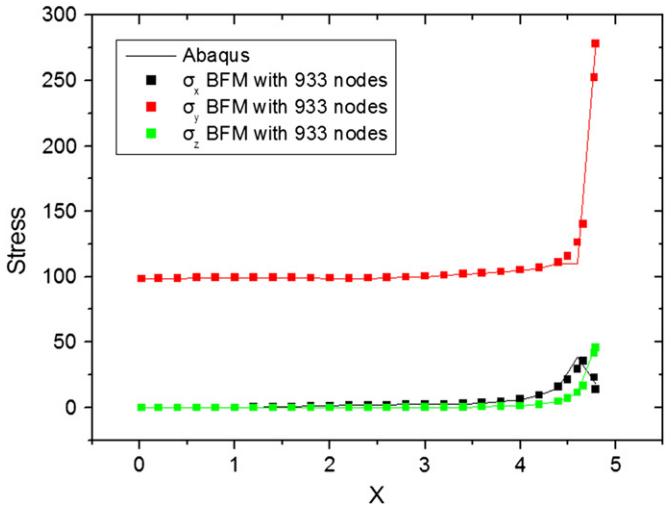

Fig. 15. Variation in stress at internal locations for a block with 5 holes of diameter 0.4.

elements and nodes are 301 and 933, respectively, while in traditional method the related numbers up to 4052 and 12,156, respectively. Even if the number of elements of the traditional method is 13 times more than the proposed method, the variation of the stress obtained by the BFM used new proposed elements is in excellent agreement with that of the traditional BFM.

In order to assess the accuracy of the proposed method, the results calculated by our method are compared to the results calculated by Abaqus. The results of stress at the internal locations are evaluated. These locations are uniformly distributed on the line with ends (0, 5, 2) and (4.8, 5, 2). In Abaqus, in order to accurately capture the stress concentration, 65,820 quadratic hexahedron elements and 280,429 nodes are used. All results are shown in Fig. 15. We can see that the variation of the stress obtained by the BFM with new proposed method is in excellent agreement with the results obtained by Abaqus. And the actual stress concentration at a point close to the surface of the hole is in very good agreement with those obtained by Abaqus.

5.3. *Block with multiple holes of arbitrary shape*

The third example is a $10 \times 10 \times 10$ block with 64 open-ended cylindrical holes of arbitrary shape, as shown in Fig. 16(a). This example is more geometrically complicated. It is considered here to show the advantage of our method in modeling of structures containing many open-ended tubular holes of arbitrary shape. The BFM boundary meshes with proposed elements are shown in Fig. 16(b). Surfaces of this complicated structure are discretized with only 1980 boundary elements and 7860 nodes. Three slender tube elements are used for each tube. It is very difficult to obtain a reasonable discretization with domain elements used in the FEM for this example. Much effort is also required to discretize all surfaces with high quality boundary elements used in the traditional BFM. And much more elements are used by the traditional BFM. However, it is very easy to describe tubular holes and their ends with proposed elements.

In this example, the Young's modulus is 1 and the Poisson's ratio is 0.25. The elastic stress problems are solved in which the essential boundary conditions are imposed on all faces corresponding to a cubic exact solution. And this solution is expressed as:

$$u_x = -2x^2 + 3y^2 + 3z^2$$
$$u_y = 3x^2 + -2y^2 + 3z^2$$

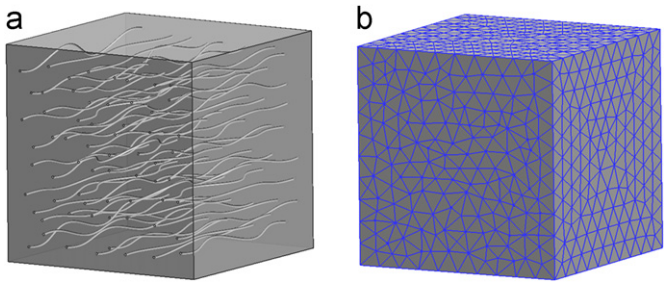

Fig. 16. (a) A block with 64 open-ended cylindrical holes; (b) BFM meshes with proposed elements.

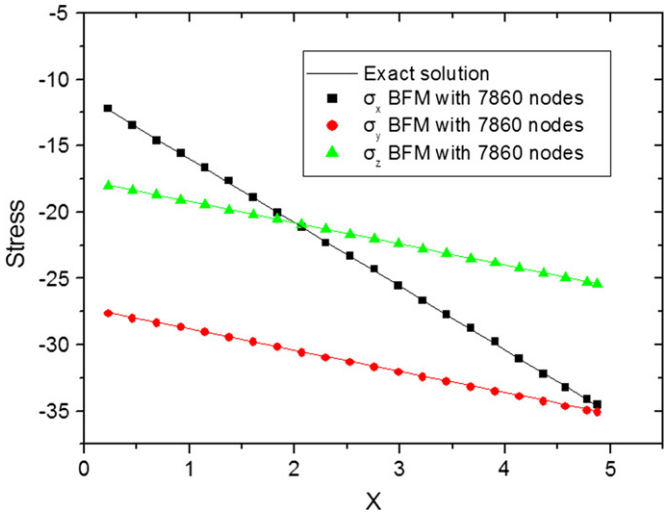

Fig. 17. Variation in stress at internal locations for a block with 64 open-ended cylindrical holes of arbitrary shape.

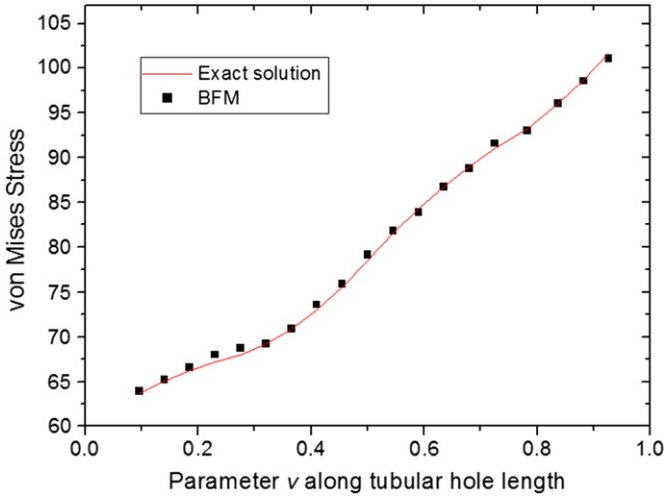

Fig. 18. Variation in von Mises stress along the specified isoline on a tubular hole.

$$u_z = 3x^2 + 3y^2 + -2z^2 \tag{15}$$

The numerical results of stress in three dimensions at the internal location are evaluated. These locations are uniformly distributed on the line segment from (0.223, 5, 5) to (4.9, 5, 5). The numerical results together with exact solutions of the stress are shown in Fig. 17. Even if there are many holes of arbitrary shape, the numerical results are still in good agreement with the exact solutions.

In addition, boundary locations are also used as evaluation points. These locations are uniformly spaced on the isoparamertic line segments from (0.5, 0.05) to (0.5, 0.95) of a hole surface, for which two coordinate parameters u and v are set in the interval [0,1]. Fig. 18 shows the numerical results of Mises stress at the boundary locations. It is observed that numerical results are in excellent agreement with the exact solution. Even if the points are close to the tube end, the results are also very precise. We can see that the elements with negative parts around the tube ends can be used to represent the end of the holes reasonably and effectively.

6. Conclusions

A boundary face method with an effective numerical model for elastic stress analysis of solids with small open-ended tubular holes has been presented in this paper. Two types of special surface elements have been proposed to represent these holes efficiently. A free shaped hole has been represented by several tube elements, and the end faces of the hole have been modeled by several special triangular elements with negative parts. So the discretization of the domain is much simpler than the conventional BFM. Therefore, the amount of data and computational cost are considerably reduced. The BFM is implemented, thus no geometric error has been introduced. We have also developed special schemes for numerical integration over very irregular tube elements.

The accuracy and efficiency have been verified through several examples. The local stress concentration can be captured accurately by our method. It also shown that the free shaped tubular holes can be exactly modeled by a few of proposed elements. Thus, the present method is especially applicable for analysis of the solids with many free shaped tubular holes.

Acknowledgements

This work was supported in part by National Science Foundation of China under grant numbers 10972074 and 11172098, in part by National 973 Project of China under grant number 2010CB328005, and in part by project under grant number 2011ZX04003–011.

References

[1] Henry DP, Banerjee PK. Elastic analysis of three-dimensional solids with small holes by BEM. Int J Numer Methods Eng 1991;31:369–84.
[2] Banerjee PK, Henry DP. Elastic analysis of three-dimensional solids with fiber inclusions by BEM. Int J Solids Struct 1992;29:2423–40.
[3] Chatterjee J, Henry DP, Ma F, Banerjee PK. An efficient BEM formulation for three-dimensional steady-state heat conduction analysis of composites. Int J Heat Mass Transfer 2008;51:1439–52.
[4] Ma F, Chatterjee J, Henry DP, Banerjee PK. Transient heat conduction analysis of 3D solids with fiber inclusions using the boundary element method. Int J Numer Methods Eng 2008;73:1113–36.
[5] Dargush GF, Banerjee PK. Advanced development of the boundary element method for steady-state heat conduction. Int J Numer Methods Eng 1989;28:2123–43.
[6] Barone MR, Caulk DA. Special boundary integral equations for approximate solution of potential problems in three-dimensional regions with slender cavities of circular cross section. IMA J Appl Math 1985;35:311–25.
[7] Federico C Buroni, Rogerio J Marczak, A family of hole boundary elements for modeling materials with cylindrical voids, engineering analysis with boundary elements. 008; 32: 78-590.
[8] Jianming Zhang Xianyun Qin, Xu han, Guangyao Li. A boundary face method for potential problems in three dimensions. Int J Numer Methods Eng 2009;80(3):320–37.

[9] Xianyun Qin, Jianming Zhang, Guangyao Li, Xiaomin Sheng, Qiao Song and Donghui Mu. An element implementation of the boundary face method for 3D potential problems, Engineering Analysis with boundary elements. 010, 34: 934–43.
[10] Zhang JM, Yao ZH, Li H. A hybrid boundary node method. Int J Numer Methods Eng 2002;53:751–63.
[11] Zhang JM, Yao ZH. Meshless regular hybrid boundary node method. Comput Model Eng Sci 2001;2:307–18.
[12] Miao Y, Wang YH, Yu F. Development of hybrid boundary node method in two dimensional elasticity. Eng Anal Boundary Elem 2005;29:703–12.
[13] Miao Y, Wang Y, Wang YH, Meshless A. Hybrid boundary node Method for Helmholtz problems. Eng Anal Boundary Elem 2009;33(2):120–7.